$LiCoO_2$ and SnO_2 Thin Film Electrodes for Lithium-Ion Battery Applications

J. P. Maranchi,[1] A.F. Hepp[2], and P. N. Kumta,[1,*]

[1]*Department of Materials Science and Engineering, Carnegie Mellon University, Pittsburgh, PA 15213 USA*

[2]*Photovoltaic & Space Environments Branch, NASA Glenn Research Center, Cleveland, OH 44135*

z E-mail: kumta@cmu.edu

Abstract

There is an increasing need for small dimension, ultra-lightweight, portable power supplies due to the miniaturization of consumer electronic devices. Rechargeable thin film lithium-ion batteries have the potential to fulfill the growing demands for micro-energy storage devices. However, rechargeable battery technology and fabrication processes have not kept pace with the advances made in device technology. Economical fabrication methods lending excellent microstructural and compositional control in the thin film battery electrodes have yet to be fully developed. In this study, spin coating has been used to demonstrate the flexiblility of the approach to produce both anode (SnO_2) and cathode ($LiCoO_2$) thin films. Results on the microstructure, crystal structure, and electrochemical properties of the thin film electrodes are described and discussed.

Keywords

$LiCoO_2$; SnO_2; spin coating; microstructure; thin film battery; economical

1. Introduction

Thin film batteries have become desirable energy storage devices for the diverse group of consumer portable devices and space related government applications. Sputtering, chemical vapor deposition (CVD), and evaporation have often been used to fabricate the various components of thin film batteries. Kanehori *et al.* [1] used all three to develop a prototype thin film battery in the early 1980's. In the 1990's, sputtering and evaporation were used to produce commercially feasible thin film lithium batteries of type Li metal|solid electrolyte|(TiS_2 or $LiMn_2O4$) [2]. Thin film lithium and lithium-ion batteries incorporating thin film $LiCoO_2$ cathodes were also produced by sputtering and evaporation [3-7]. Although the performance of the thin film batteries recently fabricated by physical vapor deposition (PVD) methods has been satisfactory, economical and versatile processing techniques are desirable to reduce the cost and improve microstructural and compositional control of the thin film electrodes.

Spin coating is a viable technique that is easy and relatively economical due to the reduced real estate and instrumentation. It can be used to produce a wide variety of electrochemically active cathode thin films. V_2O_5 thin films fabricated by spin coating on Ni/Si substrates were found to reversibly cycle greater than 3 equivalents of Li^+ per unit of V_2O_5.[8] The spin coating approach was also used to prepare thin films of $LiMn_2O_4$ for use as a cathode material in thin film batteries.[9] Other lithium containing transition metal oxide compounds such as $LiMn_xNi_{1-x}O_2$, $LiMn_{2-x}Co_xO_4$, and $LiNi_{1-x}Co_xO_2$ were also synthesized by a spin coating method, but were not evaluated electrochemically.[10] Similarly, Kushida *et al.* used sol-gel science and spin coating to produce $LiCoO_2$ thin films on Si substrates, but they did not investigate the electrochemical properties of the films.[11] Electrical resistivity and cyclic

voltammetry analyses of spin coated $LiCoO_2$ thin films on glass and aluminum foil substrates were conducted by Ehrlich *et al.*[12] A variety of precursor formulations designed to enhance wetting during spin coating were used to produce $LiCoO_2$ films on Pt/Ti coated Si substrates. The sol-gel produced films showed larger grain size and better electrochemical properties with increasing final anneal temperature.[13] A sol-gel spin coating process incorporating a crack preventing component, poly(vinylpyrrolidone), in the precursor solution was used to produce $LiCoO_2$ thin films on Au and quartz substrates which showed good electrochemical properties.[14]

Spin coating has not been widely used to produce anode thin films for lithium-ion batteries. However, low-pressure chemical vapor deposition has been used to produce thin films of SnO_2 which cycled well out to ~120 cycles.[15,16] The electrochemical properties of sputter deposited SnO_2 anode thin films were investigated by Nam *et al.*[17] Electron beam evaporation has also been used to fabricate thin film SnO_2 and Si doped SnO_2 anodes.[18]

Following these initial studies on SnO_2 and $LiCoO_2$, spin coating has been used in this study to synthesize cathode and anode films. $LiCoO_2$ thin films on both stainless steel and gold coated alumina substrates were synthesized. Thin films of SnO_2 on stainless steel were also synthesized. The properties of the electroactive thin film materials were examined using x-ray diffraction, scanning electron microscopy, and electrochemical cycling. The advantages of using a gold coated alumina substrate rather than a stainless steel substrate for the cathode current collector are discussed. The morphological change of the SnO_2 thin film due to electrochemical cycling is also discussed. Although the fabrication techniques described in this paper have not been optimized, the results show the potential of using spin coating methods to synthesize high quality anode and cathode films for thin film lithium-ion batteries.

2. Experimental

2.1 Cathode Synthesis

Spin coating was used in this study as depicted in Figure 1. Thin films of $LiCoO_2$ were synthesized on stainless steel and gold coated alumina substrates using the procedure shown in Figure 2. The 304 stainless steel substrates (Goodfellow) were punched and flattened 1 cm^2 disks 0.125 mm thick. The Superstrate S41-41 alumina substrates (Coorstek) were 1 mm thick as received and were cut into 0.8 cm x 0.8 cm squares. The alumina substrate was coated with gold using thermal evaporation on two sides and at least two edges. Electrical continuity from the face to the obverse was checked using a Fluke multimeter. Stoichiometric amounts of lithium acetate dihydrate (99.999%, Aldrich) and cobalt acetate tetrahydrate (98+%, Aldrich) were dissolved in anhydrous methanol (99.8%, Aldrich) to make a 1 mM solution. 1 mL of precursor solution was pipetted onto the substrate per deposition. Typical spin coating parameters were a spin speed of 3000 rpm and a spin time of 30 s. Immediately following the spin coating procedure, the sample was transferred to a 100°C hotplate for 1 minute to remove any remaining methanol followed by a 1 minute 525°C anneal in

air on a homemade, resistive heating pyrolysis station with embedded thermocouple. The procedure was repeated until the desired amount of electrode material was achieved. In this study, an empirical approach was employed to determine the approximate number of spin coating depositions necessary to achieve ultimate reversible capacities in the 50-100 $\mu Ah/cm^2$ range. A final air anneal was performed at 800°C in a tube furnace for 10 minutes to achieve the polycrystalline high T $LiCoO_2$ phase. A semi-rapid thermal annealing procedure was adopted for the final anneal in which a quartz sled was preheated to 800°C, then pulled to the end of the open tube where the sample was placed in the center of the sled, and finally the sled was pushed back into the hot zone of the tube furnace for the 10 minute anneal in standing air. A typical number of deposition steps to fabricate a thin film cathode was 30.

2.2 Anode Synthesis

Thin films of SnO_2 were synthesized on stainless steel substrates as shown in Figure 3. The stainless steel disks were prepared in the same fashion mentioned above in the Cathode Synthesis section. A dilute solution of colloidal tin (IV) oxide in water was prepared from the as-received ammonia stabilized colloidal suspension (Alfa). The as-received solution was a 15% dispersion of SnO_2 in water and it was further diluted using the volumetric ratio, as-received colloidal SnO_2 : distilled H_2O = 2:5. 1 mL of precursor solution was pipetted onto the substrate per deposition. Typical spin coating parameters were a spin speed of 3000 rpm and a spin time of 30 s. Immediately following the spin coating procedure, the sample was transferred to a 150°C hotplate for 2 minutes to remove any remaining water and then placed directly onto a preheated 400°C resistively heated, thermocouple embedded heating station in air for 5 minutes to remove any residual ammonia. The procedure was repeated until achieving the desired amount of electrode material. An empirical method was used to determine the number of spin coat depositions necessary to achieve ~ 40-100 $\mu Ah/cm^2$ of reversible capacity. A typical number of depositions to fabricate a thin film anode was 3.

2.3 Characterization of Electrodes

2.3.1 Phase Analysis

X-ray diffraction (XRD) was used to perform phase analyses on the substrates and as-prepared thin film electrodes. The instrument used in this study incorporated a state-of-the-art detector (XRD, Philips PW3040PRO, θ/θ powder diffractometer with X'celerator detector and Cu radiation source). Two-theta scans were typically taken from 10° to 90° with a step size of 0.05°.

2.3.2 Microstructural Analysis

The microstructure of the films was examined using a scanning electron microscope (FEG-SEM, Philips XL30) and a contact mode atomic force microscope (AFM, Veeco).

2.3.3 Electrochemical Analysis

The electrochemical properties of the thin film electrodes were examined using a conventional 3 electrode type cell as shown in Figure 4. The samples were all dried in a vacuum oven for at least 12 hours at 105°C and placed inside an argon filled glove box (Vacuum Atmospheres, Hawthorn, CA, < 10 ppm O_2 and H_2O) for fabrication of half-cells. The half-cells were fabricated in the glove box using lithium foil and a glass fiber separator (Whatman GF/D) together with the electrode films and 1 M $LiPF_6$ in ethylene carbonate/dimethyl carbonate (2:1) electrolyte (Merck). The 3 electrode cells were placed in desiccant jars with electrical feedthroughs, removed from the glove box, and allowed to equilibrate for 12 hours prior to galvanostatic cycling (Arbin Instruments). All charge/discharge experiments had the cycling voltages limited between 20 mV-1.2V and 3.1V-4.2V for the anodes and cathodes, respectively. The $LiCoO_2$ on stainless steel experiment was performed at a current density of 100 $\mu A \cdot cm^{-2}$ (corresponding to ~ C/1.2 rate) while the $LiCoO_2$ on gold coated alumina experiment used a current density of 31.25 $\mu A \cdot cm^{-2}$ (corresponding to ~ C/2.5 rate). The SnO_2 on stainless steel experiment was carried out at a current density of 40 $\mu A \cdot cm^{-2}$ (corresponding to ~ 1C rate). All of the tests included a 60 s rest between each charge or discharge half cycle.

3. Results and Discussion

3.1 $LiCoO_2$ Thin Films on Stainless Steel

The XRD of the stainless steel substrate and 30 spin (30S) sample are shown together in Figures 5a and 5c, respectively. The XRD pattern for 30S shows $R\bar{3}m$ phase $LiCoO_2$ with peaks matching JCPDS Pattern (82-0340)[19]. After confirming the presence of $LiCoO_2$, SEM was used to determine the morphology of the as-prepared films as shown in Figure 6. Slight porosity is seen in the as-prepared film along with hexagonally faceted grains 500 nm or less in diameter. Following the investigation of the microstructure of the as-prepared film, the sample was dried well and prepared for half-cell cycling. The capacity versus cycle number for the 1st ten cycles of the galvanostatic test are shown in Fig. 7 along with the corresponding coulombic efficiency. One can see that in the first charge, the capacity is ~ 325 μAh. However, the discharge capacity in the 1st cycle drops to ~ 110 μAh, corresponding to a coulombic efficiency of only 36%. In subsequent cycles, the coulombic efficiency gradually increases to ~ 85% by the 10th cycle. The poor coulombic efficiency in the first few cycles indicated that although lithium ions could be de-intercalated from the $LiCoO_2$, a much lower amount of lithium was able to be intercalated back into the host structure. We suspect that there could be an adverse reaction between the film and the substrate, or the film itself could be highly defective.

Post-cycling SEM results of the same sample are shown in Figure 8. Figure 8a shows that the post-cycled film exhibits two distinct regions, a light region and a dark region. The light region seems to be more narrow and interconnected than the larger dark regions. Close-up views of the light and dark regions are seen in Figures 8b and 8c, respectively. The light region appears to be very similar in nature to the pre-cycled morphology shown in Figure 6b, while the dark region appears to have substantially larger grains

containing many micro-cracks. There are several possible explanations for the differences in microstructure. One possible explanation is that one of the regions has become electrically insulated from the current collector due to interfacial film formation. For example, if the light region became electrically insulated during the 800°C annealing step, the material directly above may not cycle at all and appear exactly as it did prior to electrochemical cycling. Furthermore, if one assumes that the dark region is still in good electrical contact with the current collector, it would experience a much higher current density due to the decrease in active area. The excessive current density could lead to significant intragranular stresses, micro-cracking, and grain growth as seen in Figure 8c. Micro-cracking and other deleterious cycling related effects were also seen by Wang et al.[20,21] After forming the aforementioned hypothesis, the researchers decided to intentionally form an "interfacial" phase by only depositing 10 layers of $LiCoO_2$ precursor followed by a longer 1 h anneal in air. The researchers hoped that XRD could detect some impurity phase formation. The XRD pattern of the long annealed sample is shown in Figure 5b. Upon careful indexing of the resultant peaks using the JCPDS database, the following phases were identified: Li_2CO_3, Li_3CrO_4, Fe_3O_4, $CoFe_2O_4$, $CoCr_2O_4$, $LiCoO_2$, and stainless steel. Therefore, it is reasonable to suspect that similar impurity phases were also present in the 30S sample, leading to the poor performance of the cathode.

3.2 $LiCoO_2$ Thin Films on Gold Coated Alumina

After observing the poor performance of the thin film cathode on stainless steel, it was desirable to change substrate materials. A good choice, one adopted in previous work by Neudecker et al[22], seemed to be gold coated alumina. XRD of the gold coated alumina substrate and 30A sample are shown together in Figures 9a and 9b, respectively. Other than substrate peaks, the only peaks indexed were the (003), (104), and (002) rhombohedral $LiCoO_2$ peaks. The microstructure of the uncycled $LiCoO_2$ film is seen in Figure 10. The film appears to be dense and composed of modestly faceted, high aspect ratio grains with diameters less than 1 μm. The surface topology of the uncycled film is shown in the AFM images of Figures 11a and 11b. One can see that the film is not very smooth, probably due to the nature of the alumina substrate. The capacity versus cycle number for thirty cycles of the galvanostatic test are shown in Fig. 12a along with the corresponding coulombic efficiency, Fig. 12b. One can see that in the first charge, the capacity is ~ 58 μAh. The discharge capacity in the 1st cycle drops to ~ 50 μAh, corresponding to a good 1st cycle coulombic efficiency of 86%, much better than the 36% seen for the stainless steel substrate sample. By the 5th cycle, the coulombic efficiency had increased to ~ 97%, the steady value observed for each susbsequent cycle up to 30 cycles. Fig. 13a shows the post-cycled plan view SEM of the $LiCoO_2$ film. The morphology of the film appears to be unchanged from that shown in the pre-cycling SEM shown previously in Fig. 10. The cross-sectional view of the post-cycled $LiCoO_2$ film on gold coated alumina is shown in Fig. 13b. The cross-sectional image shows that although the film has a rough surface, it is still a continuous film with no obvious cracking in the film's bulk. The film thickness is estimated to be ~1 μm from Fig. 13b. After being satisfied with the improvements made by

utilizing a different substrate for the $LiCoO_2$ cathode, the focus shifted towards examination of the electrochemical properties of spin coated SnO_2 thin films.

3.3 SnO_2 Thin Films on Stainless Steel

Fig. 14a and 14b show the XRD patterns of an uncoated stainless steel substrate and SnO_2 coated stainless steel, respectively. From the XRD pattern, three broad, low intensity peaks were identified corresponding to SnO_2. The broad peaks indicate the nanocrystalline nature of the SnO_2 thin film. The small grain size is a result of the precursor colloidal solution (~15 nm SnO_2 particles), low heat treatment temperature, and short annealing time. The SEM image of the uncycled SnO_2 thin film is shown in Fig. 15. From the SEM image, one can see that the SnO_2 thin film is continuous, with only a few small cracks or voids. The actual grain size of the SnO_2 thin film can be estimated at ~ 20-50 nm as shown in the height AFM image of Fig. 16. The results of the half-cell galvanostatic cycling experiment performed on the SnO_2 thin film are shown in Fig. 17. The capacity versus cycle data and corresponding coulombic efficiencies are shown in Figs. 17a and 17b, respectively. Although the first cycle irreversible loss is quite high (~70%), the remaining cycles have a steady capacity up to the 20^{th} cycle. About 50% of the initial capacity is expected to be lost in the case of materials like SnO_2 due to the large consumption of Li in the irreversible formation of Li_2O. In an attempt to explain the extra capacity loss, post-cycle SEM on the SnO_2 thin film was performed after the 20^{th} cycle. The SEM result is shown in Fig. 18. It appears that regions of the film have peeled, while other regions (for example, the area above the scale marker on the right side of the image) have remained well-adhered to the substrate. The large scale morphological change in the SnO_2 film caused by the well-known volume expansion/contraction phenomenon experienced by Sn based anode materials is the most likely source of the unusually high irreversible loss observed.

4. Conclusion

In this paper, spin coating has been shown to be a viable, economical processing method for the production of both cathode and anode thin films for lithium-ion batteries. The importance of substrate selection on the electrochemical properties of spin coated $LiCoO_2$ thin films has been emphasized. The choice of a stainless steel substrate led to poor cycling performance accompanied by the formation of intragranular micro-cracks during cycling. A careful XRD study identified several impurity phases which could be responsible for the poor cycling performance in the case of the stainless steel substrate. Conversely, gold coated alumina proved to be a good choice for the substrate. The $LiCoO_2$ thin film on Au-alumina had low 1^{st} cycle irreversible loss and cycled well for the 30 cycle experiment. Spin coated SnO_2 thin films on stainless steel substrates showed higher than normal irreversible capacity in the 1^{st} cycle. However, the good capacity retention of the SnO_2 thin films up to the 20^{th} cycle indicates their potential for use as anodes in thin film lithium-ion batteries. Spin coating has been shown to be an effective fabrication method for synthesizing good quality

cathodes and anodes for thin film lithium-ion batteries. Spin coating can be used as a processing technique in the future to produce doped lithiated transition metal oxides, samples for in-situ AFM electrode investigations, and studies on the substrate/active material interface.

Acknowledgements

J.P.M. and P.N.K. acknowledge the support of NASA (GSRP and NAG3-2640), Chang's Ascending (Taiwan), NSF (CTS-0000563), and ONR(Grant N00014-00-1-0516). The authors also acknowledge useful technical discussions with Dr. George E. Blomgren.

References

[1] K. Kanehori, K. Matsumoto, K. Miyauchi and T. Kudo, Solid State Ionics 9/10 (1983) 1445.

[2] S.D. Jones, J.R. Akridge and F.K. Shokoohi, Solid State Ionics 69 (1994) 357.

[3] J.B. Bates, N.J. Dudney, G.R. Gruzalski, R.A. Zuhr, A. Choudhury, C.F. Luck, and J.D. Robertson, Journal of Power Sources 43-44 (1993) 103.

[4] J.B. Bates, G.R. Gruzalski, N.J. Dudney, C.F. Luck, and X. Yu, Solid State Ionics 70/71 (1994) 619.

[5] J.B. Bates, N.J. Dudney, D.C. Lubben, G.R. Gruzalski, B.S. Kwak, X. Yu, and R.A. Zuhr, Journal of Power Sources 54 (1995) 58.

[6] J.B. Bates, N.J. Dudney, B. Neudecker, A. Ueda, and C.D. Evans, Solid State Ionics 135 (2000) 33.

[7] B.J. Neudecker, N.J. Dudney, and J.B. Bates, Journal of the Electrochemical Society 147(2) (2000) 517.

[8] S. Passerini, D. Chang, X. Chu, B. Dinh, and W. Smyrl, Chemistry of Materials 7(4) (1995) 780.

[9] Y.J. Park, J.G. Kim, M.K. Kim, H.T. Chung, W.S. Um, M.H. Kim, and H.G. Kim, Journal of Power Sources 76(1) (1998) 41.

[10] S. Nieto-Ramos, M.S. Tomar, S. Hernandez, and F. Aliev, Thin Solid Films 377-378 (2000) 745.

[11] K. Kushida and K. Kuriyama, Journal of Crystal Growth 237-239 (2002) 612.

[12] G.M. Ehrlich and D.M. Schleich, Sensors and Actuators A 51 (1995) 17.

[13] M.K. Kim, H.T. Chung, Y.J. Park, J.G. Kim, J.T. Son, K.S. Park, and H.G. Kim, Journal of Power Sources 99 (2001) 34.

[14] Y.H. Rho, K. Kanamura, and T. Umegaki, Journal of The Electrochemical Society 150(1) (2003) A107.

[15] T. Brousse, R. Retoux, U. Herterich, and D.M. Schleich, Journal of The Electrochemical Society 145(1) (1998) 1.

[16] R. Retoux, T. Brousse, and D.M. Schleich, Journal of The Electrochemical Society 146(7) (1999) 2472.

[17] S.C. Nam, Y.S. Soon, W.I. Cho, B.W. Cho, H.S. Chun, and K.S. Yun, Journal of The Electrochemical Society 148(3) (2001) A220.

[18] Y.I. Kim, W.H. Lee, H.S. Moon, K.S. Ji, S.H. Seong, and J.W. Park, Journal of Power Sources 101(2001) 253.

[19] JCPDS Pattern 82-0340, International Centre for Diffraction Data, Newtown Square, PA, USA.

[20] H. Wang, Y. Jang, B. Huang, D.R. Sadoway, and Y. Chiang, Journal of Power Sources 81–82(1999) 594.

[21] H. Wang, Y. Jang, B. Huang, D.R. Sadoway, and Y. Chiang, Journal of The Electrochemical Society 146(2) (1999) 473.

[22] B.J. Neudecker, N.J. Dudney, and J.B. Bates, Journal of The Electrochemical Society 147(2) (2000) 517.

Figure Captions

1. Schematic depicting the spin coating process.

2. Flowchart showing the synthesis of thin film $LiCoO_2$ cathodes on rigid substrates.

3. Flowchart outlining the synthesis of thin film SnO_2 anodes on rigid substrates.

4. "Hockey-puck" cell used for electrochemical characterization.

5. XRD of (a) stainless steel substrates (unannealed), (b) stainless steel/$LiCoO_2$ thin film (10S/final anneal), and (c) stainless steel/$LiCoO_2$ thin film (30S/final anneal).

6. SEM image of as-prepared $LiCoO_2$ thin film on stainless steel (30S/final anneal) at (a) 11266x and (b) area outlined by black rectangle in (a) at 45063x.

7. Half-cell battery cycling test of $LiCoO_2$ thin film on stainless steel (30S/final anneal). (a) Capacity versus cycle number and (b) coulombic efficency versus cycle number.

8. SEM image of galvanostatically cycled (10 cycles) $LiCoO_2$ thin film on stainless steel (30S/final anneal) at (a) 800x; (b) area I outlined by black rectangle in (a) at 25600x; and (c) area II outlined by black rectangle in (a) at 25600x.

9. XRD of (a) gold/alumina substrate (unannealed) and (b) $LiCoO_2$ thin film on gold/alumina (30A/final anneal).

10. SEM image of as-prepared $LiCoO_2$ thin film on gold/alumina (30A/final anneal) at 24569x.

11. Contact AFM images of as-prepared $LiCoO_2$ thin film on gold/alumina (30A/final anneal), 5 μm x 5 μm scan area, (a) top view and (b) surface plot.

12. Half-cell battery cycling test of $LiCoO_2$ thin film on gold/alumina (30A/final anneal). (a) Capacity versus cycle number and (b) coulombic efficency versus cycle number.

13. SEM image of galvanostatically cycled (30 cycles) $LiCoO_2$ thin film on gold/alumina (30A/final anneal) at (a) 19388x; and (b) cross-section, 16012x.

14. XRD of (a) stainless steel substrate (unannealed) and (b) SnO_2 thin film on stainless steel (3S/final anneal).

15. SEM image of as-prepared SnO_2 thin film on stainless steel (3S/final anneal) at 76242x.

16. Contact AFM image of as-prepared SnO_2 thin film on stainless steel (3S/final anneal), 375 nm x 375 nm scan area, top view.

17. Half-cell battery cycling test of SnO_2 thin film on stainless steel (3S/final anneal). (a) Capacity versus cycle number and (b) coulombic efficiency versus cycle number.

18. SEM image of galvanostatically cycled (20 cycles) SnO_2 thin film on stainless steel (3S/final anneal) at 76049x.

Figure 1

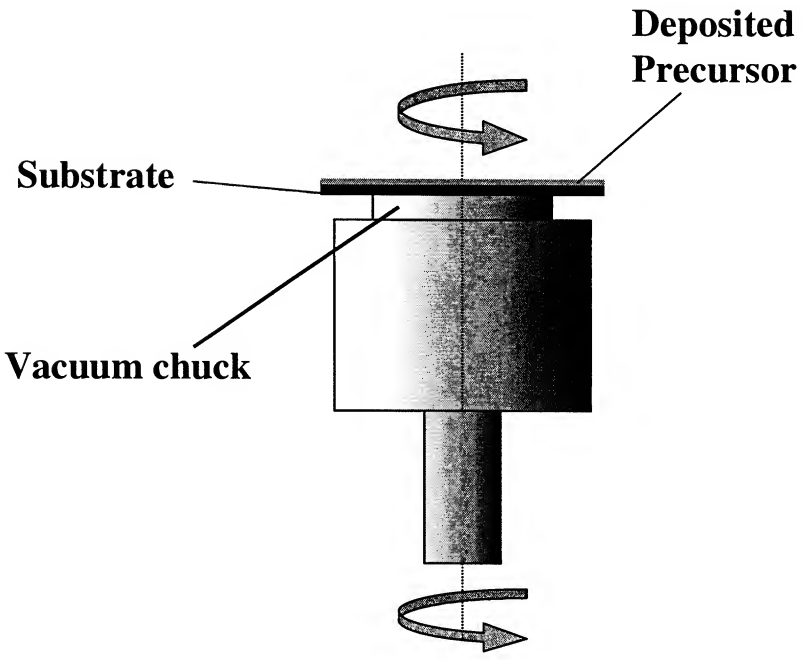

Figure 2

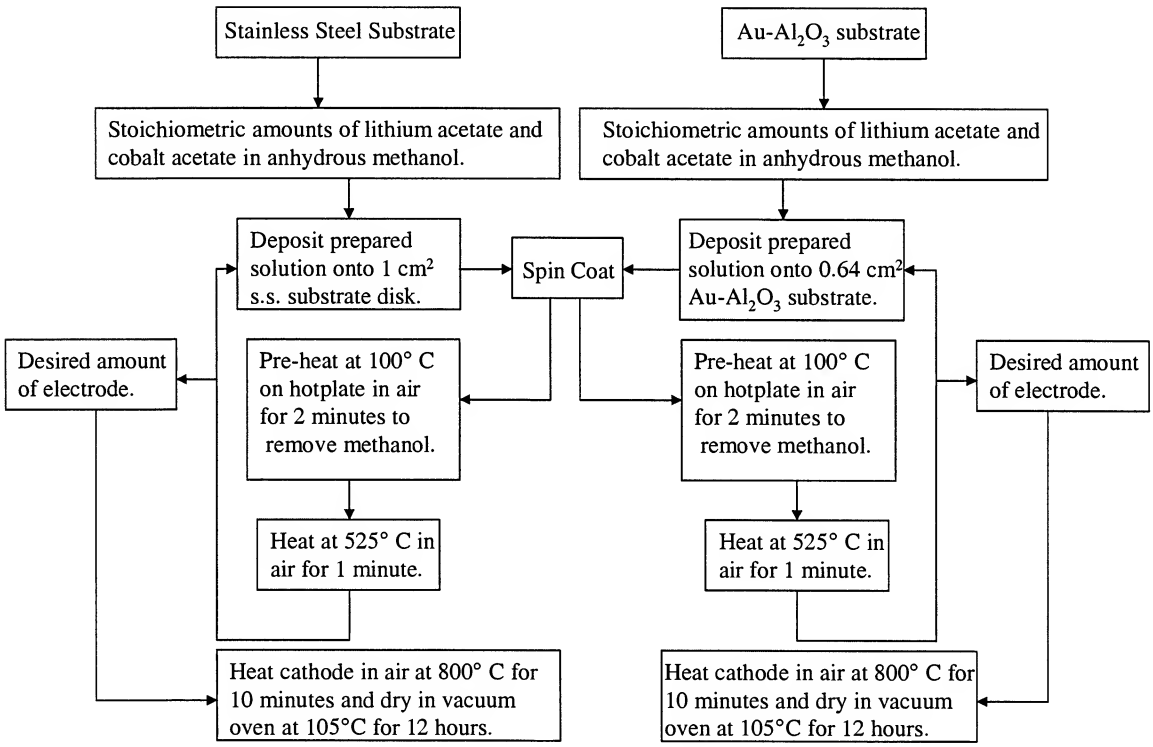
Stainless Steel Substrate
Au-Al2O3 substrate
Stoichiometric amounts of lithium acetate and cobalt acetate in anhydrous methanol.
Stoichiometric amounts of lithium acetate and cobalt acetate in anhydrous methanol.
Deposit prepared solution onto 1 cm2 s.s. substrate disk.
Spin Coat
Deposit prepared solution onto 0.64 cm2 Au-Al2O3 substrate.
Desired amount of electrode.
Pre-heat at 100° C on hotplate in air for 2 minutes to remove methanol.
Pre-heat at 100° C on hotplate in air for 2 minutes to remove methanol.
Desired amount of electrode.
Heat at 525° C in air for 1 minute.
Heat at 525° C in air for 1 minute.
Heat cathode in air at 800° C for 10 minutes and dry in vacuum oven at 105°C for 12 hours.
Heat cathode in air at 800° C for 10 minutes and dry in vacuum oven at 105°C for 12 hours.

Figure 3

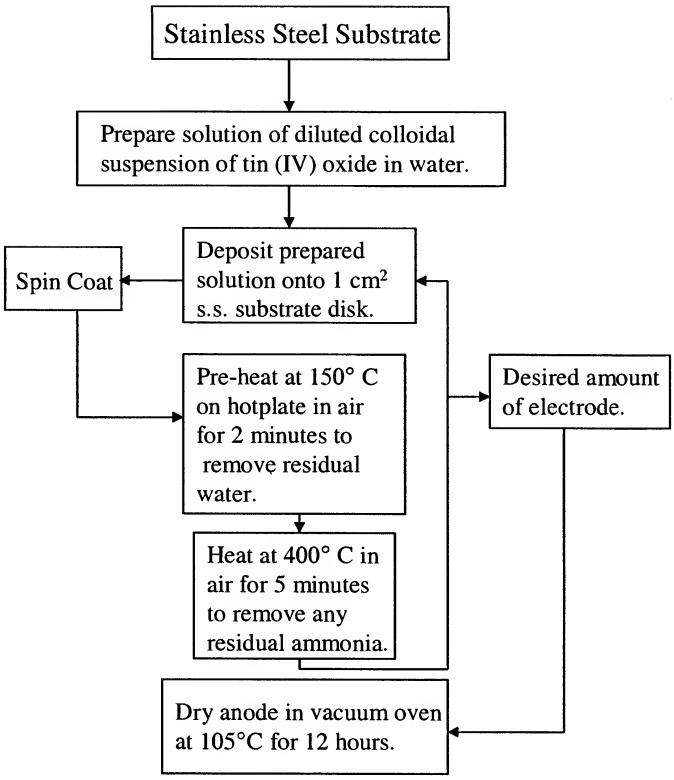
Stainless Steel Substrate
Prepare solution of diluted colloidal suspension of tin (IV) oxide in water.
Deposit prepared solution onto 1 cm2 s.s. substrate disk.
Spin Coat
Pre-heat at 150° C on hotplate in air for 2 minutes to remove residual water.
Heat at 400° C in air for 5 minutes to remove any residual ammonia.
Desired amount of electrode.
Dry anode in vacuum oven at 105°C for 12 hours.

Figure 4

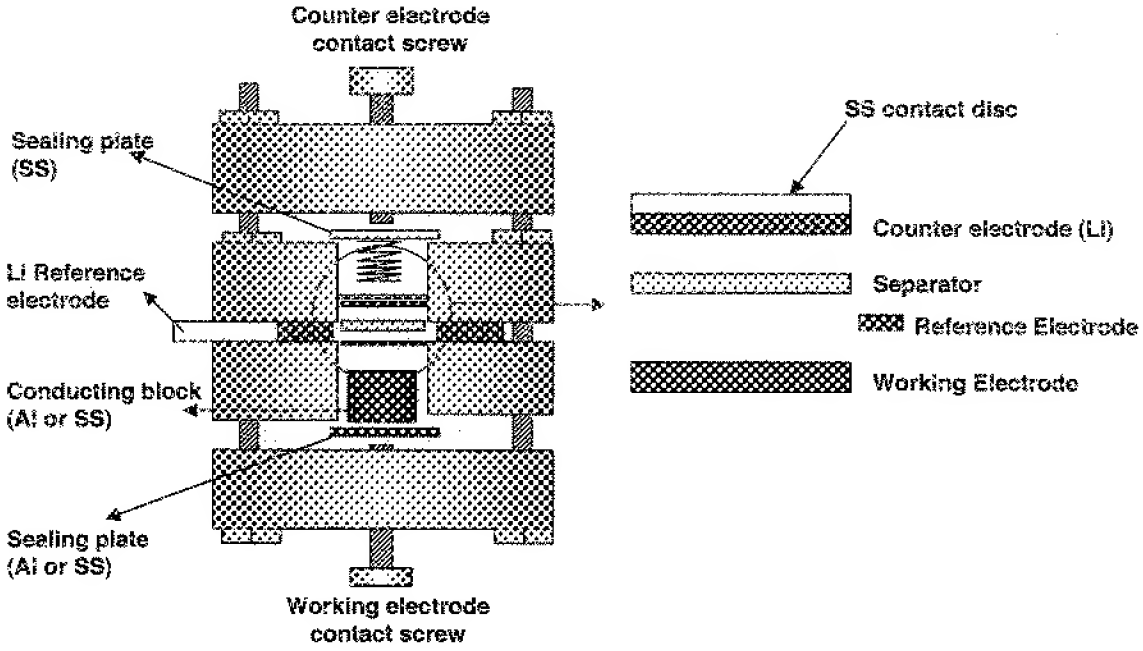
Counter electrode
contact screw
Sealing plate
(SS)
Li Reference
electrode
Conducting block
(Al or SS)
Sealing plate
(Al or SS)
Working electrode
contact screw
SS contact disc
Counter electrode (Li)
Separator
Reference Electrode
Working Electrode

Figure 5

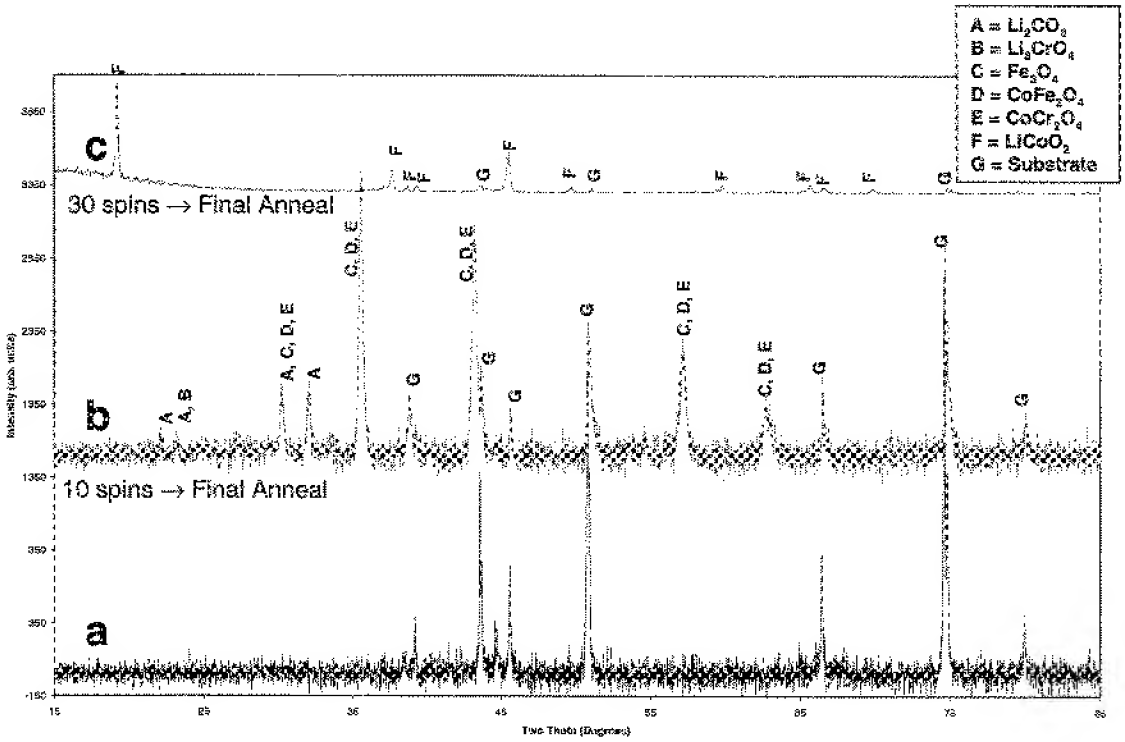
A = Li_2CO_3
B = Li_2CrO_4
C = Fe_3O_4
D = $CoFe_2O_4$
E = $CoCr_2O_4$
F = $LiCoO_2$
G = Substrate
c
30 spins → Final Anneal
b
10 spins → Final Anneal
a
Intensity (arb. units)
Two Theta (Degrees)

Figure 6

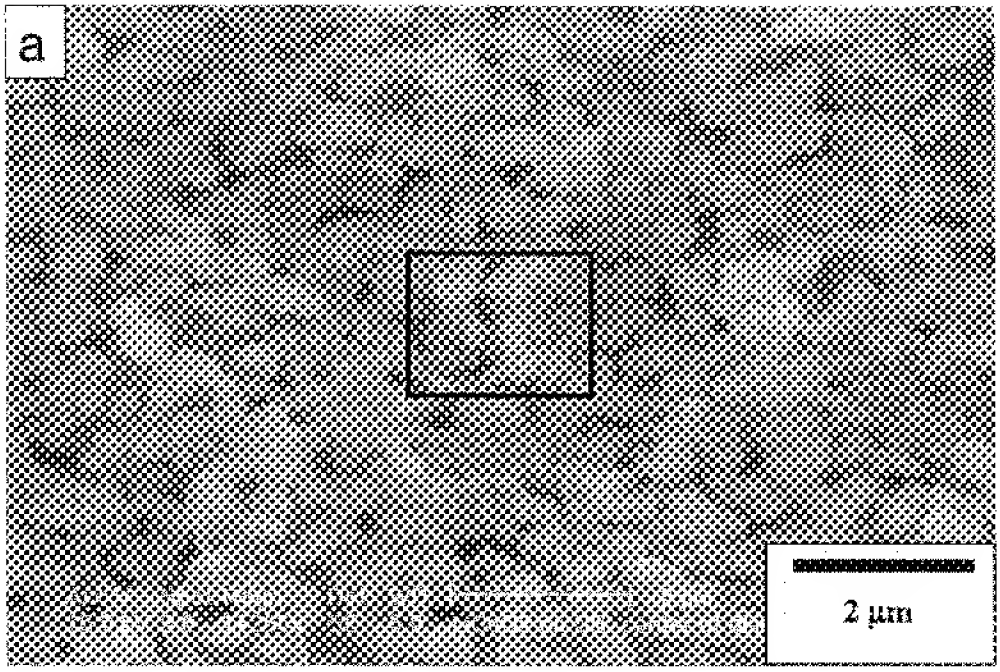

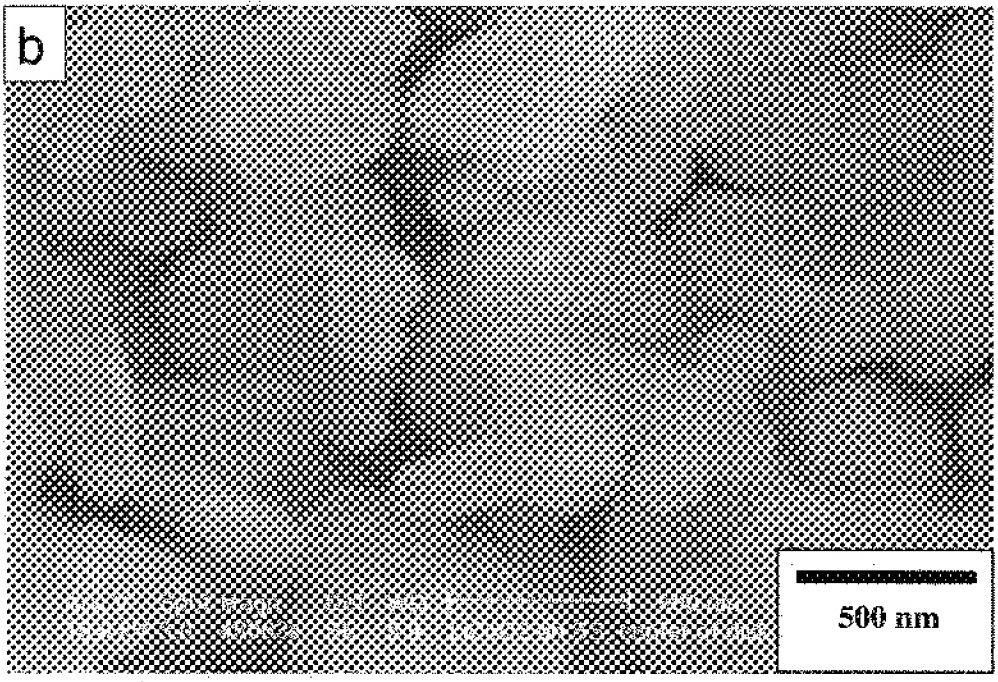

Figure 7

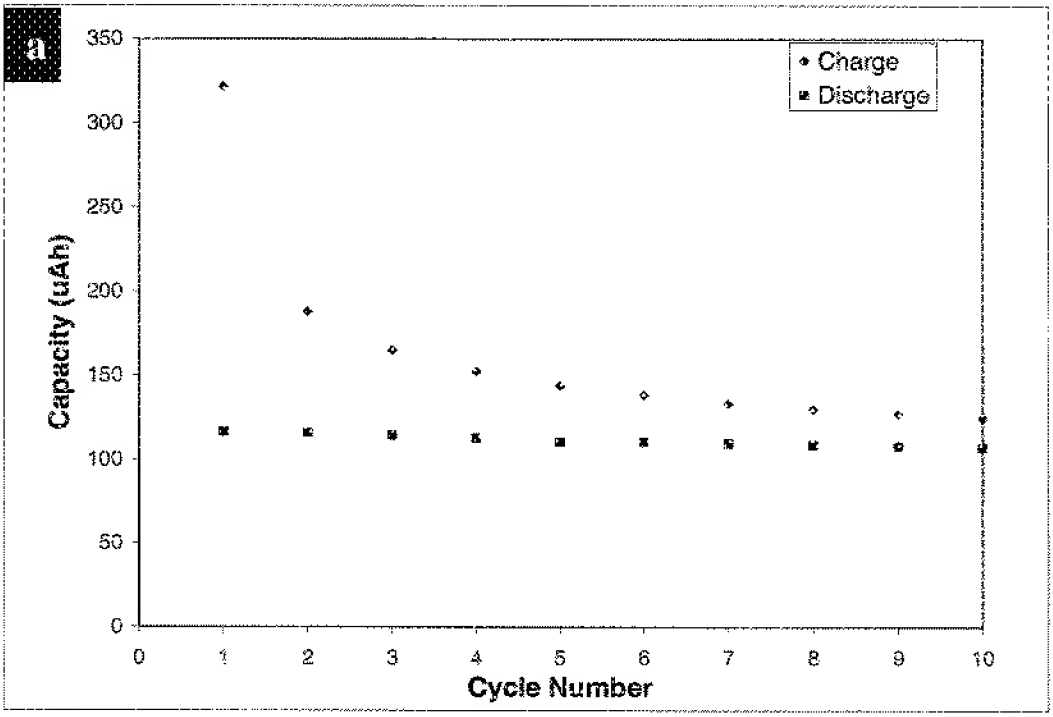
a
Charge
Discharge
Capacity (uAh)
Cycle Number
0
50
100
150
200
250
300
350
0
1
2
3
4
5
6
7
8
9
10

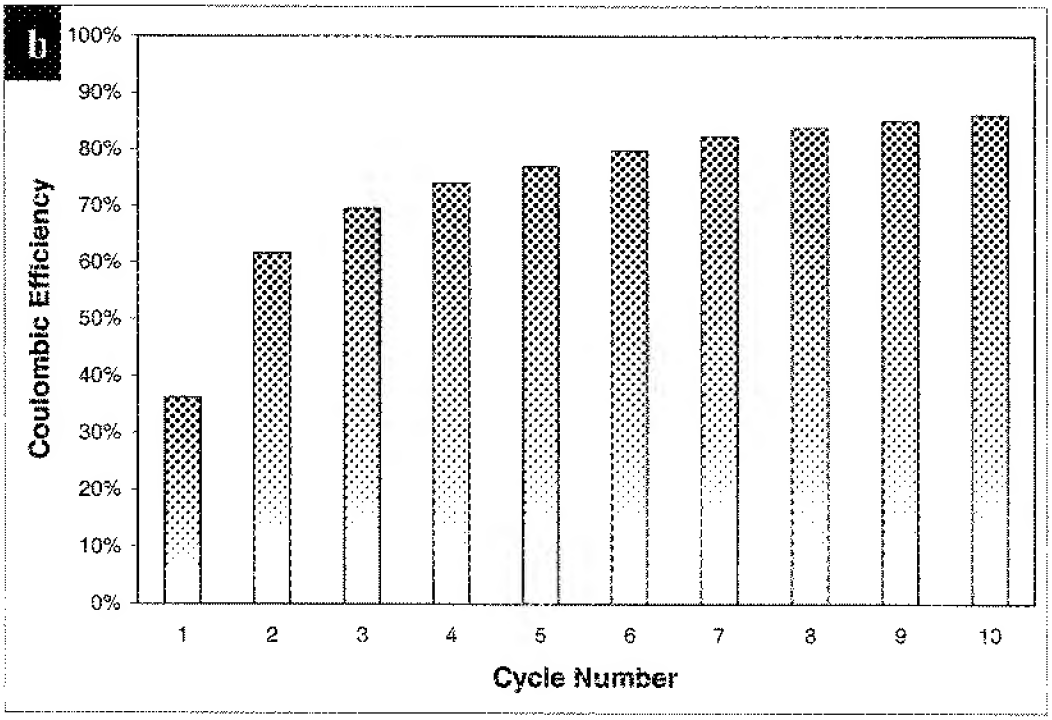
b
Coulombic Efficiency
Cycle Number
0%
10%
20%
30%
40%
50%
60%
70%
80%
90%
100%
1
2
3
4
5
6
7
8
9
10

Figure 8

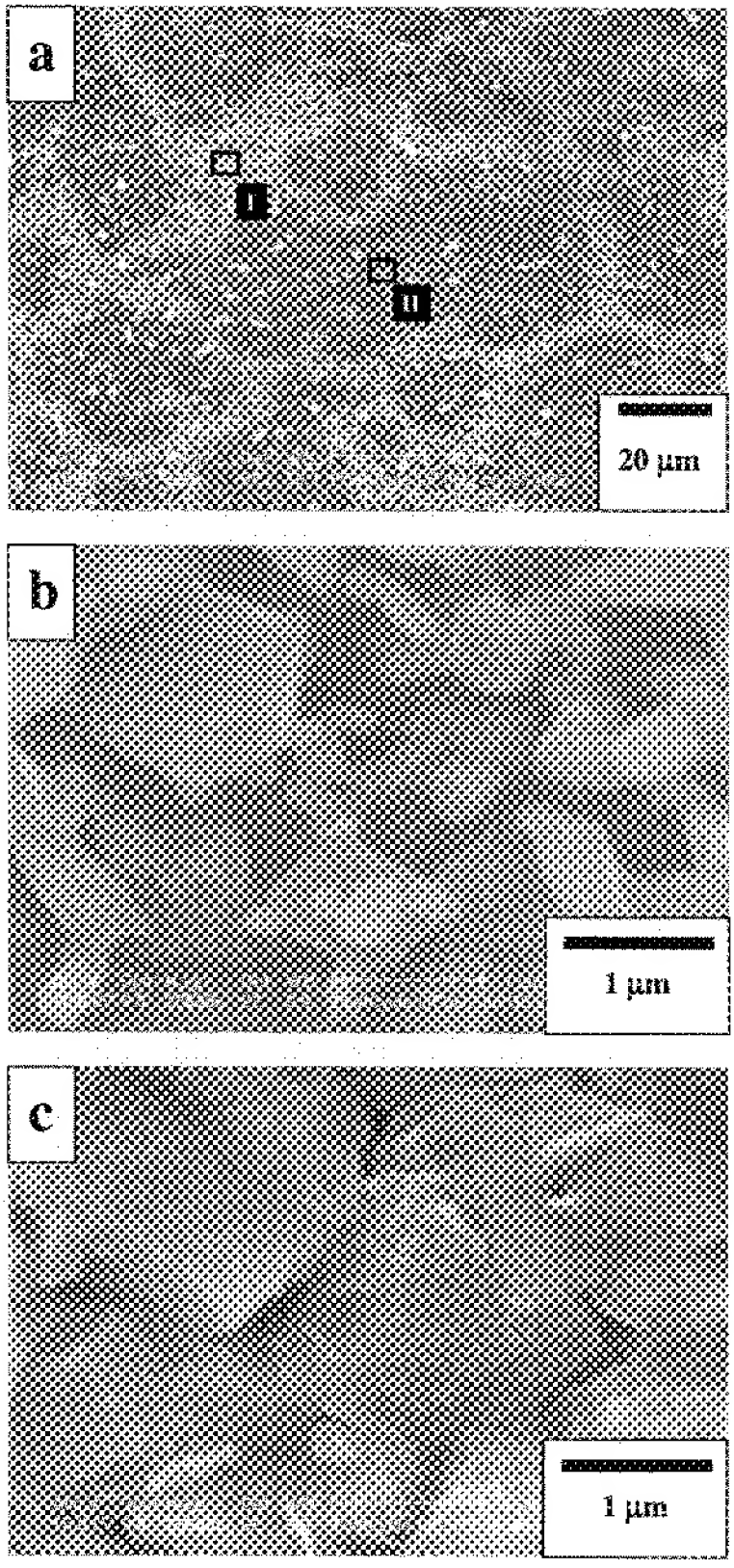

Figure 9

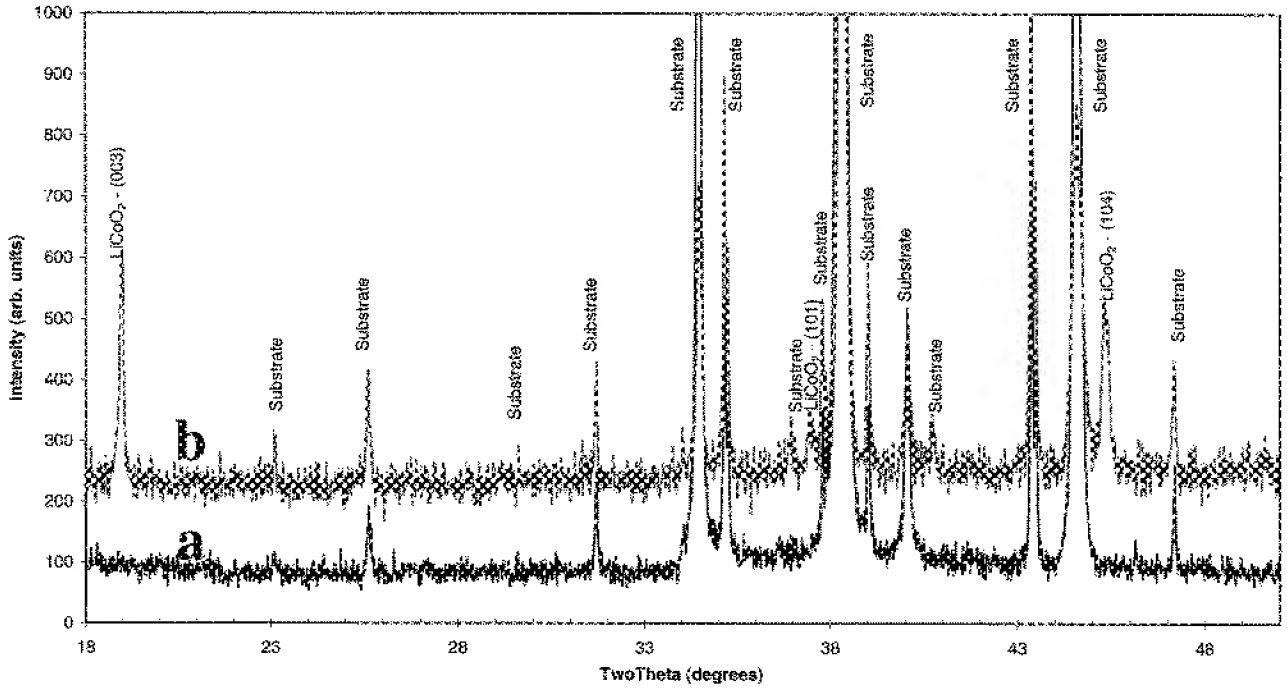
Intensity (arb. units)
TwoTheta (degrees)
LiCoO2 - (003)
LiCoO2 - (101)
LiCoO2 - (104)
Substrate
a
b

Figure 10

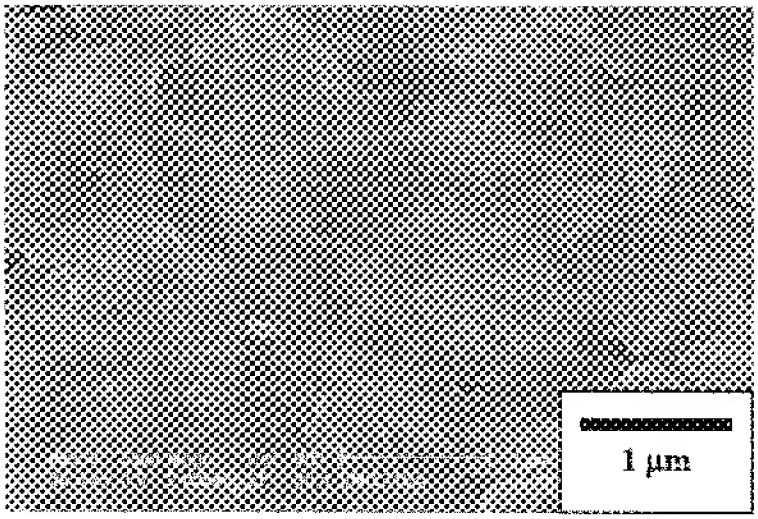

Figure 11

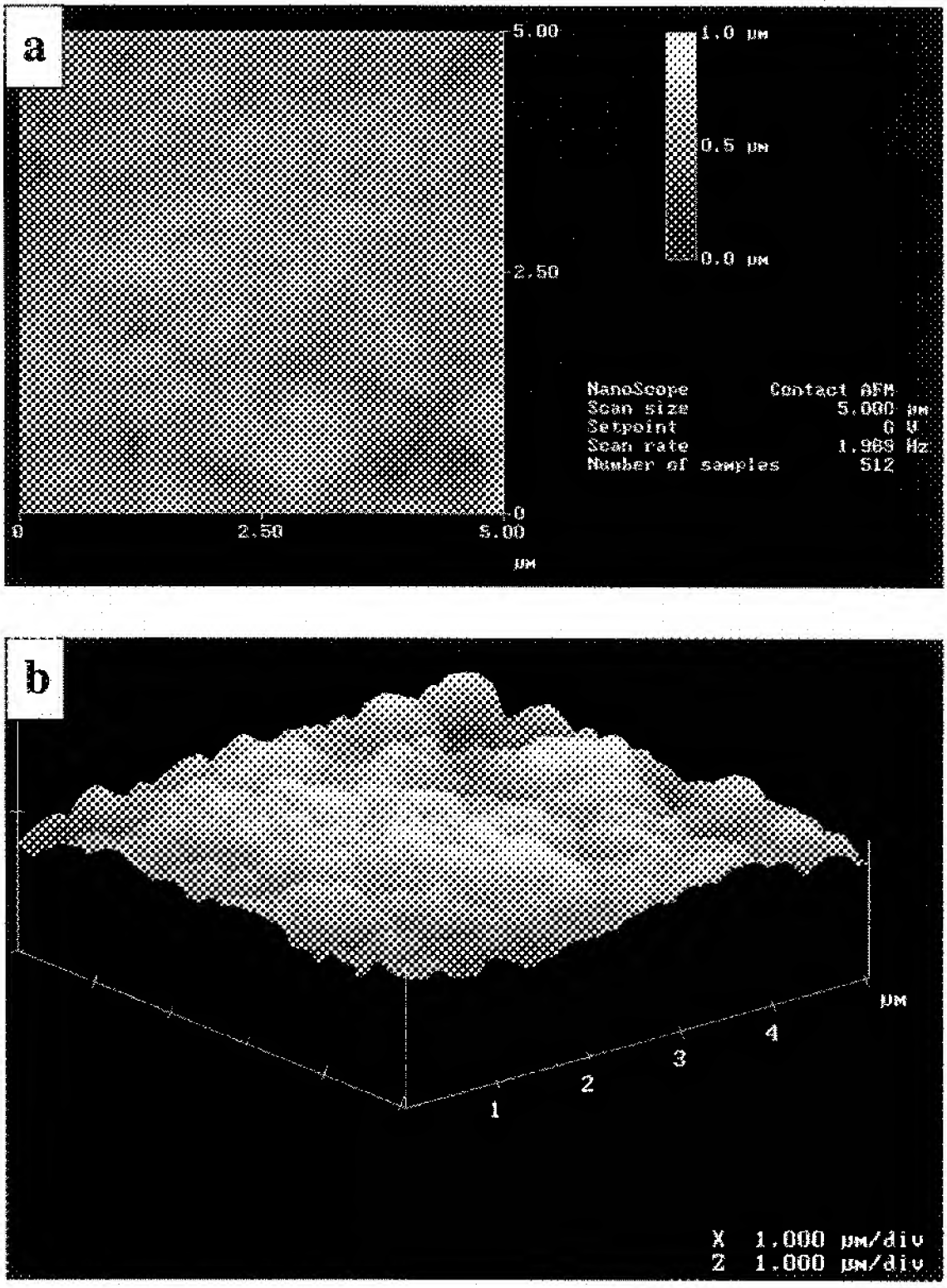
a
5.00
2.50
0
0
2.50
5.00
μm
1.0 μm
0.5 μm
0.0 μm
NanoScope Contact AFM
Scan size 5.000 μm
Setpoint 0 V
Scan rate 1.969 Hz
Number of samples 512
b
μm
1
2
3
4
X 1.000 μm/div
Z 1.000 μm/div

Figure 12

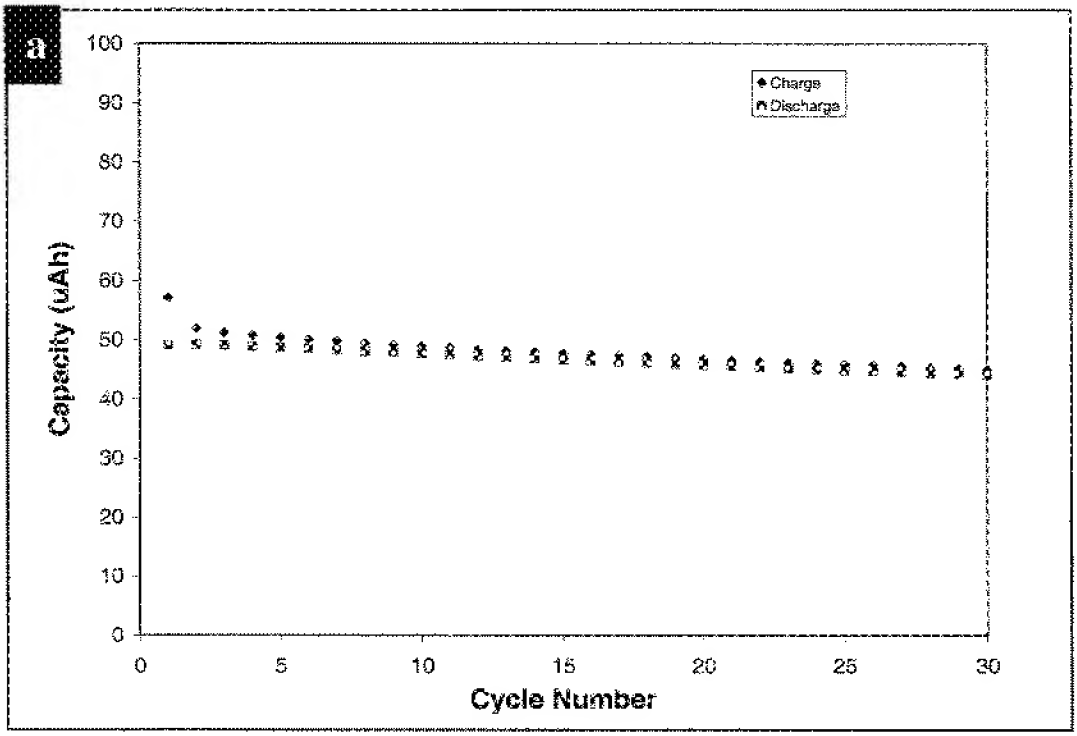
a
Capacity (uAh)
Cycle Number
Charge
Discharge
0
10
20
30
40
50
60
70
80
90
100
0
5
10
15
20
25
30

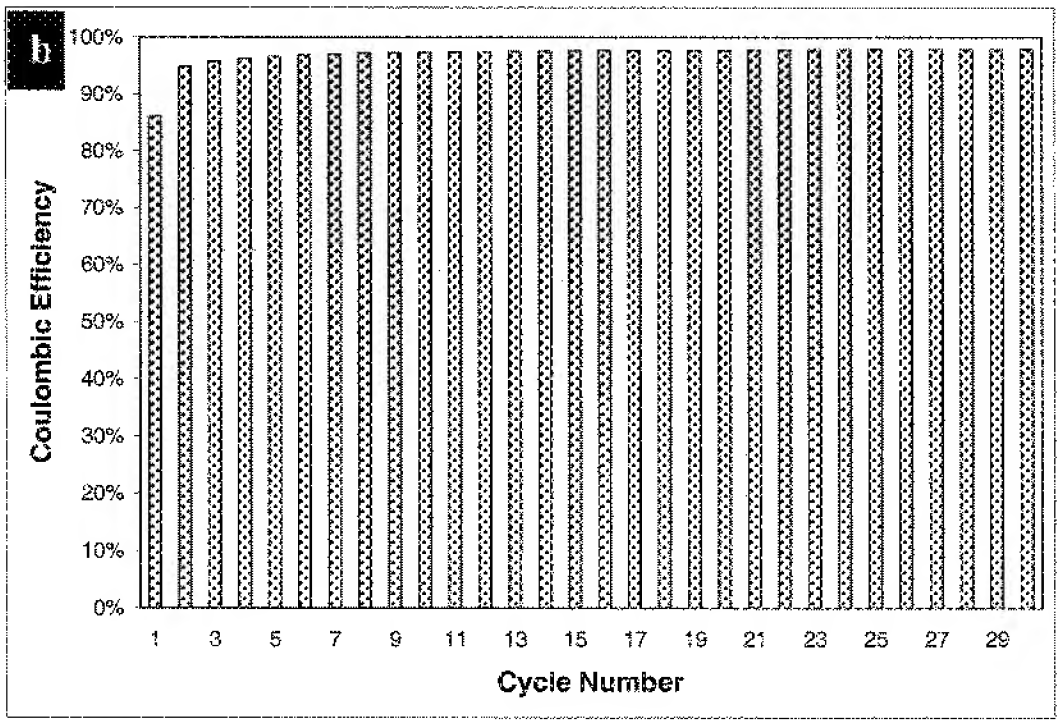
b
Coulombic Efficiency
Cycle Number
0%
10%
20%
30%
40%
50%
60%
70%
80%
90%
100%
1
3
5
7
9
11
13
15
17
19
21
23
25
27
29

Figure 13

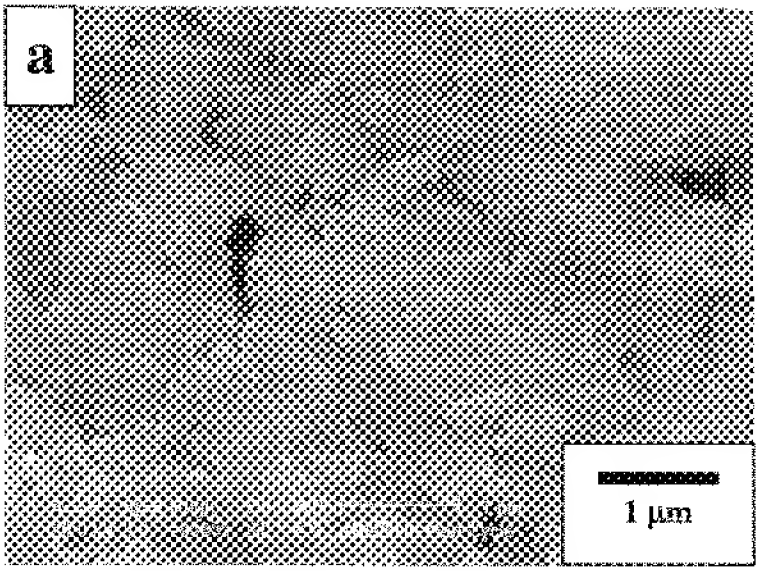

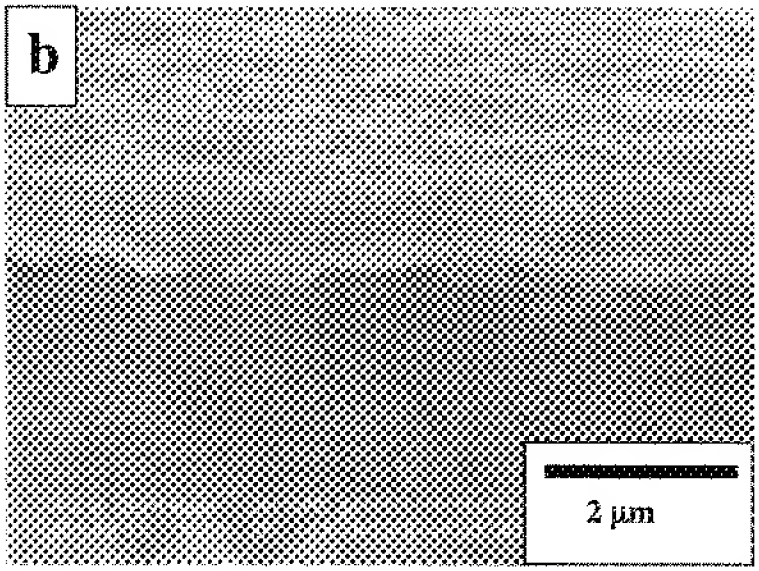

Figure 14

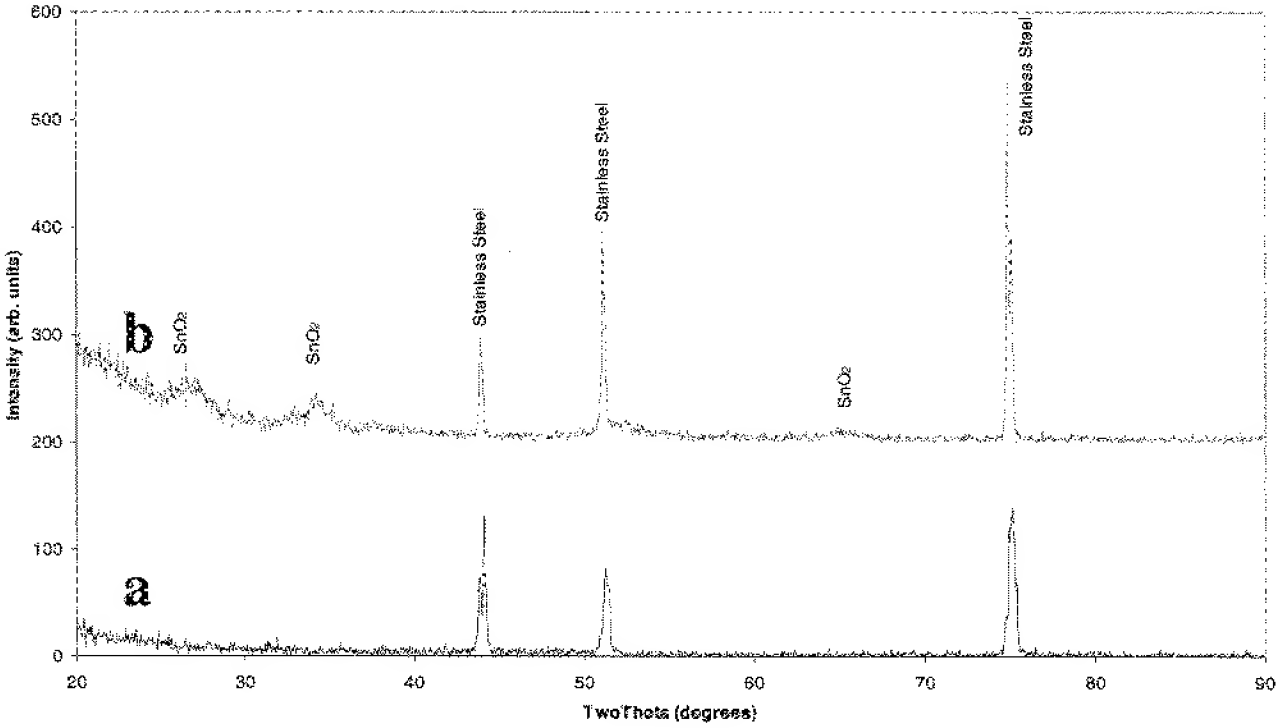
Intensity (arb. units)
TwoTheta (degrees)
b
a
SnO2
SnO2
Stainless Steel
Stainless Steel
SnO2
Stainless Steel

Figure 15

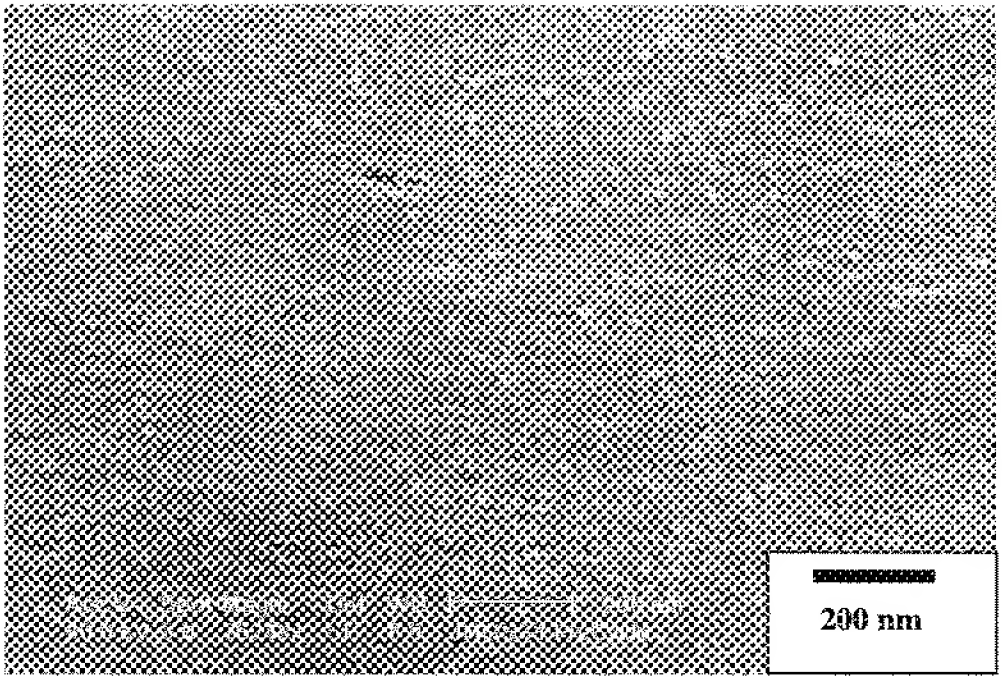

Figure 16

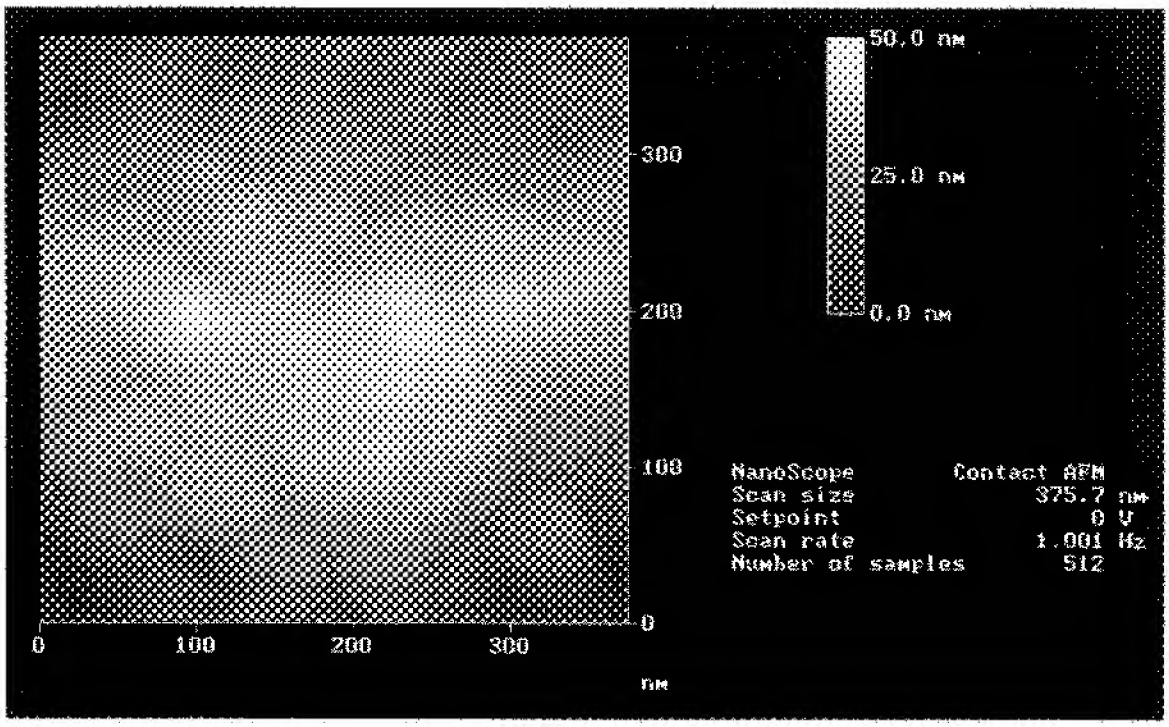
50.0 nm
25.0 nm
0.0 nm
300
200
100
0
0
100
200
300
nm
NanoScope
Contact AFM
Scan size
375.7 nm
Setpoint
0 V
Scan rate
1.001 Hz
Number of samples
512

Figure 17

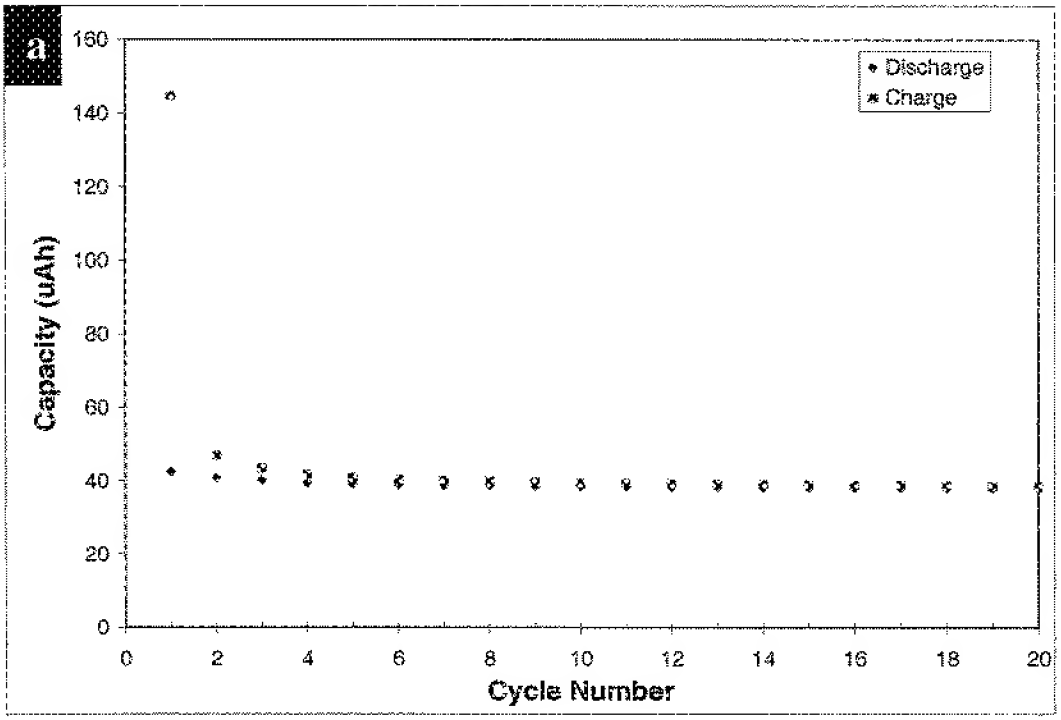
a
Discharge
Charge
Capacity (uAh)
Cycle Number
0
20
40
60
80
100
120
140
160
0
2
4
6
8
10
12
14
16
18
20

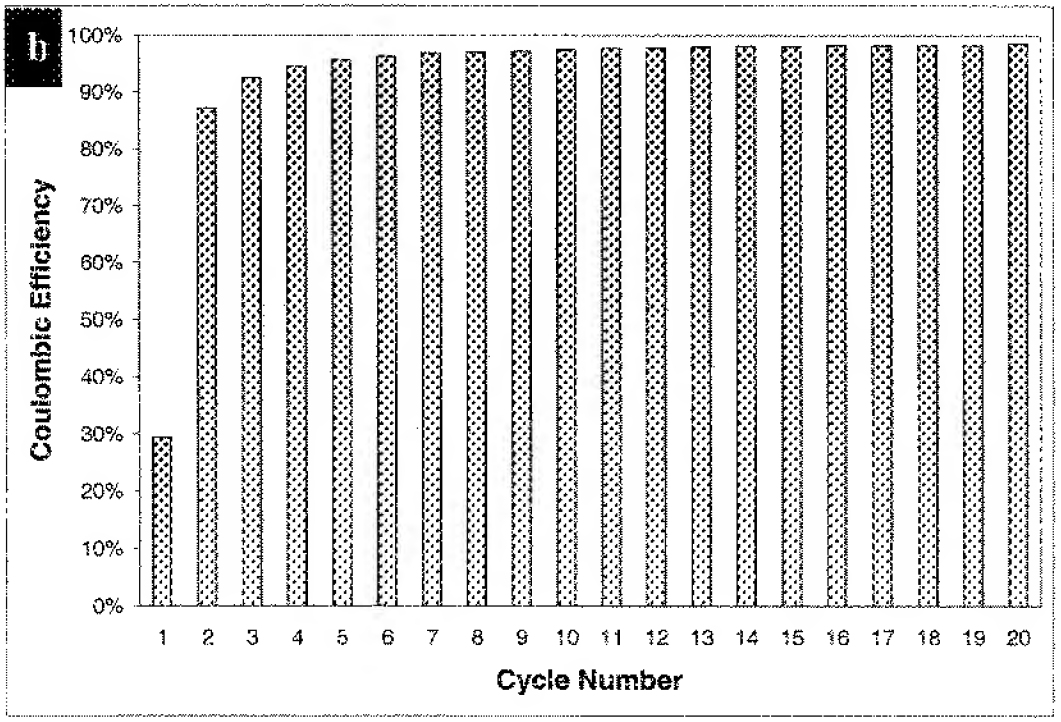
b
Coulombic Efficiency
Cycle Number
0%
10%
20%
30%
40%
50%
60%
70%
80%
90%
100%
1
2
3
4
5
6
7
8
9
10
11
12
13
14
15
16
17
18
19
20

Figure 18